Sampling Errors of SSM/I and TRMM Rainfall Averages: Comparison with Error Estimates from Surface Data and a Simple Model

THOMAS L. BELL, PRASUN K. KUNDU,* AND CHRISTIAN D. KUMMEROW

Laboratory for Atmospheres, NASA Goddard Space Flight Center, Greenbelt, Maryland

Manuscript submitted May 2000 to *J. Appl. Meteor.*

* SM&A Corporation (East), 2600 Park Tower Drive, Suite 1000, Vienna, VA 22180

Corresponding author address: Dr. Thomas L. Bell, Code 913, Goddard Space Flight Center, Greenbelt, MD 20771. E-mail: <Thomas.L.Bell@gsfc.nasa.gov>.

ABSTRACT

Quantitative use of satellite-derived maps of monthly rainfall requires some measure of the accuracy of the satellite estimates. The rainfall estimate for a given map grid box is subject to both remote-sensing error and, in the case of low-orbiting satellites, sampling error due to the limited number of observations of the grid box provided by the satellite. A simple model of rain behavior predicts that rms random error in grid-box averages should depend in a simple way on the local average rain rate, and the predicted behavior has been seen in simulations using surface rain-gauge and radar data. This relationship was examined using satellite SSM/I data obtained over the western equatorial Pacific during TOGA COARE. RMS error inferred directly from SSM/I rainfall estimates was found to be larger than predicted from surface data, and to depend less on local rain rate than was predicted. Preliminary examination of TRMM microwave estimates shows better agreement with surface data. A simple method of estimating rms error in satellite rainfall estimates is suggested, based on quantities that can be directly computed from the satellite data.

---

1. Introduction

Satellite data are now regularly used to produce gridded maps of rainfall averaged over time intervals ranging from hours to many months. It has not been easy, however, to provide accompanying quantitative estimates of the accuracies of the grid-point averages. This is in part because remote-sensing techniques do not yet provide sufficient information to allow unambiguous conversion of measurements into rain-rate values for the observed area, and the distribution of errors introduced in the conversion depends on the observed situation in ways that are not always known. The problem is exacerbated by the highly intermittent character of rain, which makes averages of rain data noisy and comparison of remote-sensing results with measurements made on the ground difficult.

The Tropical Rainfall Measuring Mission (TRMM) satellite was launched in 1997. Descriptions of TRMM are given by Simpson et al. (1988, 1996) and Kummerow et al. (1998). One of the primary goals of the mission is to provide rain data sufficiently accurate that TRMM satellite products can serve as a kind of transfer standard to calibrate rain estimates from other satellite systems and thereby improve the overall accuracy of global rain maps. To help reach this goal, the satellite carries several instruments on board including a precipitation radar and a passive microwave sensor, the latter having higher resolution than most satellite-borne microwave instruments.

An important component of the effort towards reaching this goal is developing quantitative estimates of the accuracy of the gridded products of TRMM. A number of different approaches to this are being tried, including development of models for the error intrinsic to the remote sensing methods themselves; comparison of satellite products to ground-based measurements from rain-gauge arrays, radar sites, and aircraft measurements during field campaigns; and comparison with other satellite observations.

Although much can be learned about sources of error in the TRMM rain estimates from examining individual overlapping coincident snapshots of rain events

taken by various TRMM instruments and by other satellites and ground-based observation systems, much can also be learned from comparisons among *averages* of satellite data and ground-based data. As long as the averages of the satellite estimates and ground-based or other-satellite estimates are taken from time intervals and spatial locations which are believed to have similar statistics, such averages allow enormously more data to be used in the comparisons than can be assembled from coincident observations. Comparisons of averages of data reveal biases in rain estimates. Such biases may be small compared to discrepancies found in point-by-point comparisons of coincident observations, yet knowledge of these biases is important when TRMM data are used as a transfer standard, and especially so when the data are used for climatological studies.

One of the commonest methods of comparing satellite estimates of rainfall to ground-based observations and to other satellite estimates is to test the agreement of averages over a spatial domain, such as a grid box on a map, averaged over a sufficiently long time period that the averages are stable enough for the comparison to be informative. Even if the remote-sensing techniques are perfectly accurate, such averages will contain sampling error because the systems are not measuring rainfall everywhere in the area at every moment. Rain gauges, for example, measure more or less continuously in time but cover very little of the area, whereas radar views irregular shaped volumes of the atmosphere at frequent but non-continuous intervals of time, and satellite observations are till more widely spaced in time. While averages from two different systems may disagree because of inherent errors in the measurement methods, they will almost certainly disagree because they contain different sampling errors.

Mathematically, comparison of two grid-box averages can be formulated like this: Suppose a system X—TRMM, perhaps—gives an estimate R_X for the average rainfall $\bar{R}$ in a grid box over some time interval of the order of a month or so, and that system

Y—another satellite, perhaps, or a ground-based system—gives an estimate R_Y for the same area and time. Each system makes an (unknown) error

$$\varepsilon_\alpha = R_\alpha - \bar{R}; \qquad \alpha = X, Y. \tag{1.1}$$

A portion of the error ε_α is due to possible algorithmic and instrumental errors in estimating rain rate when it is observed, or to differences in the mean rain rate observed by the two systems due to spatial or temporal inhomogeneity in the rain statistics, such as spatial variation in the mean rain rate, or a diurnal cycle. The rest is due to inadequate sampling. To compare the estimates of the two systems to see if one is biased relative to the other, one examines whether the difference $R_X - R_Y$ is bigger than can be explained by chance. A straightforward approach is typically to estimate the mean squared difference

$$\begin{aligned} \sigma^2 &= \langle (R_X - R_Y)^2 \rangle \\ &= \langle (\varepsilon_X - \varepsilon_Y)^2 \rangle \\ &= {\sigma_X}^2 + {\sigma_Y}^2 - 2\langle \varepsilon_X \varepsilon_Y \rangle \,, \end{aligned} \tag{1.2}$$

where $\sigma_\alpha^2 \equiv \langle \varepsilon_\alpha^2 \rangle$, and to estimate the bias as $R_X - R_Y \pm 2\sigma$. (The limits $\pm 2\sigma$ would be appropriate if the difference $R_X - R_Y$ is normally distributed and 95% confidence limits are wanted. If $|R_X - R_Y| > 2\sigma$, one is fairly sure that there is a nonzero bias present. See, for example, Taylor (1997) for a discussion of such approaches.)

The use of σ this way to make quantitative inferences about the bias, however, assumes that the statistics of the differences $R_X - R_Y$ are normally distributed, which cannot be taken for granted. Even when the assumption of normality is not completely justified, though, the above approach to inferring a bias is likely to be a good approximation to the correct one. A more satisfactory approach to this problem might be to collect enough data from the two systems so that the statistical distribution of the difference $R_X - R_Y$ itself could be established. Having obtained it, one could empirically determine confidence limits for the bias $\langle R_X - R_Y \rangle$, where the angular brackets indicate

an average over an ensemble of datasets similar in nature to what has been collected. An approach like this would probably benefit from employing resampling techniques. See Zwiers (1990) and Wilks (1997), however, for important caveats concerning these methods.

The more conventional approach based on (1.2) has the advantage that it is easily automated and easy to apply to disparate regions of the world, time periods, and rainfall-estimation methods. Published results of studies done by various groups are often already cast in this format so that comparisons can be quickly made. It should also be noted that the error estimates σ as defined above are exactly what are needed if a satellite map of rainfall is to be compared with climate models, whose output is generally in the form of grid-box averages. If the satellite map of $\bar{R}$ is assumed to be accurate to $\pm 2\sigma_X$ for some grid box, and the climate model forecast to be accurate to $\pm 2\sigma_Y$ (due to predictability limits), the satellite map value and the model forecast should agree to within $\pm 2\sigma$ computed from Eq. (1.2).

The purpose of this paper is to explore methods of estimating σ_X for weekly to monthly averages of rain estimates obtained from microwave instruments on low earth-orbiting satellites, including those on TRMM and the Special Sensor Microwave/Imagers (SSM/I) on Defense-Meteorological-Satellite-Program (DMSP) satellites. Because raindrops interact strongly with microwave radiation, such instruments are believed to provide some of the best estimates of rain rates observed from satellite platforms. Sampling error contributes substantially to σ_X for these satellites because they observe any spot on the earth only a few times per day at best. It was originally argued (e.g., Wilheit 1988, Bell et al. 1990) that "retrieval errors," the errors made in estimating actual rain rates from microwave measurements, might contribute relatively little to σ_X because the large number of fields of view (FOVs) averaged over in forming a monthly average would tend to produce relatively small net average retrieval error, even if

individual random retrieval errors were large. Results presented in this paper appear not to support this.

The error σ_X is likely to depend on many aspects of rain in a given region, such as the amount and types of rainfall, the average synoptic conditions, the season, sea-surface temperatures, availability of moisture, levels of aerosol contaminants, etc., as well as on the sampling and observational characteristics of the satellite and its instruments. In a previous paper, Bell and Kundu (1996), hereafter abbreviated as BK96, derived a simple formula expressing the sampling error as a function of the mean rain rate and an "effective" number of samples. A more general argument for the same formula was subsequently developed by Bell and Kundu (2000), hereafter abbreviated BK00. They tested this formula using the sampling characteristics of the TRMM satellite and the statistical properties of a number of datasets from ground-based rain-gauge and radar measurements. In this paper, we continue the investigation by comparing the formula's prediction of the behavior of rms error in monthly averages obtained from a satellite-derived dataset.

The dataset studied here contains retrieved rain rates over the western tropical Pacific during the Tropical Ocean Global Atmosphere/Coupled Ocean Atmosphere Research Experiment (TOGA COARE), during November 1992 to February 1993. The rain rates are derived from SSM/I data taken from two DMSP satellites that were orbiting at the time, the F10 and F11. The algorithm used in the retrievals is similar to but not so highly developed as the one presently being used for TRMM. Details will be given later. It is found that a fairly simple parameterization of the random error in monthly averages over 2.5° × 2.5° grid boxes seems to describe the data well, but that the dependence on the mean rain rate in the grid box is different from what was predicted by the model and observed using ground-based data as summarized in BK00, and the error magnitudes are much higher.

The source of this difference appears to be the very different responses of the satellite microwave instruments and algorithm to the presence of stratiform rain when compared with the ground-based measurements. This explanation will be discussed in a separate paper. Such a rain-type-dependent response has important implications for using one satellite estimate to calibrate another, as is sometimes done in combining datasets to produce global maps of rainfall, or in comparing satellite estimates to ground-validation datasets.

Despite the differences observed here in the random error of satellite averages compared with that of ground-based averages, the approach can still be used to obtain parameterized estimates of σ_X as a function of the average rain rate in a grid box, and thus can be used to supply fairly simple descriptions of the confidence levels to be applied to each grid-box value of rain rate generated from the satellite data. Comparisons of satellite estimates against values obtained from ground-based instruments can therefore be carried out using Eq. (1.2), provided the sampling error σ_Y in the ground-based estimates can be obtained and the covariance term $\langle \varepsilon_X \varepsilon_Y \rangle$ estimated. In many instances the covariance term can probably be neglected, either because it is actually small or because it will tend to decrease σ, so that ignoring it will mean that σ is at worst overestimated and the error bars will therefore be conservatively estimated.

In the following section we briefly review a model for how sampling error should depend on rain rate and other factors and how sampling error estimates obtained with ground-based data compare with the simple model. We describe the SSM/I-derived dataset from which estimates of the random error in SSM/I monthly averages are obtained in section 3, and in section 4 compare the estimates with estimates made from surface radar taken in tropical oceanic environments. The SSM/I statistics display a simple power-law dependence on local rain rate, and these power laws are described in section 5. In section 6 we report some preliminary results on rainfall statistics

observed by TRMM and compare and contrast them with the results from the SSM/I observations. Section 7 summarizes our results and gives some concluding remarks. Some statistical and computational details are provided in an appendix.

2. Review of a simple model for sampling error

A simple theoretical model presented in BK00 suggests how sampling error might depend on the rainfall climatology and satellite sampling characteristics for a given grid box. For the reader's convenience and to establish notation we briefly review the formula and the underlying concepts and definitions. For the detailed derivations see BK00.

a. Definitions

We are interested in an estimate of the space–time-averaged rain rate

$$\bar{R} = (1/T) \int_0^T dt R_A(t) \,, \tag{2.1}$$

where

$$R_A(t) = (1/A) \int_A d^2\mathbf{x} R(\mathbf{x}, t) \tag{2.2}$$

is the area-averaged instantaneous rain rate, $R(\mathbf{x}, t)$ is the local rain rate at the point $\mathbf{x}$ at time t, T is the averaging period, taken here to be one month, and A is the area of the grid box. We assume A to be large enough so that the rain rates in neighboring boxes can be assumed to be statistically uncorrelated to a good approximation.

The satellite in general views a grid box intermittently and even then sometimes only partially. Thus the instrument provides an estimate $\hat{R}_i$ of the rain rate at times $\{t_i, i = 1, \ldots, n\}$ averaged over an area $A_i \leq A$ corresponding to the region of overlap between the grid box and the instrument swath during the overpass at time t_i. The satellite estimate $\hat{R}$ of the true monthly average $\bar{R}$ is obtained as a weighted average of the individual estimates $\hat{R}_i$:

$$\hat{R} = \frac{1}{n} \sum_{i=1}^{n} w_i \hat{R}_i \tag{2.3}$$

with suitably chosen weights w_i normalized to

$$(1/n)\sum_{i=1}^{n} w_i = 1 \,. \tag{2.4}$$

(The estimate $\hat{R}$ would be an example of R_X in Eq. 1.1.) A convenient way to obtain $\hat{R}$ directly from the data is to average the rain-rate estimates from all the instrument footprints that fall within the area A over the period T. (If the footprints are distributed relatively uniformly over the areas A_i then such an average is equivalent to setting $w_i \propto A_i/A$. If the footprints are nonuniformly distributed but the area average $\hat{R}_i$ has been corrected for this, the same choice for w_i is appropriate. It is shown in BK96 that this choice of weights provides a near-optimal estimate of $\bar{R}$ for most grid boxes seen by TRMM except those at the highest latitudes.)

The uncertainty in the estimate $\hat{R}$ is measured by the mean squared error

$$\sigma_E^2 = \langle (\hat{R} - \bar{R})^2 \rangle \,, \tag{2.5}$$

where the angular brackets denote an average over an ensemble of rain scenarios consistent with the local rainfall climatology. In general, as discussed in BK00, σ_E^2 contains contributions from both the sampling error arising from intermittent satellite coverage and the retrieval error arising from the errors in converting the results of measurements into actual rain rates. If we can assume that the retrieval errors are uncorrelated from footprint to footprint, the contribution of these errors to $\hat{R}$ tends to be small (Wilheit 1988; Bell et al. 1990), and the total error σ_E^2 is dominated by the sampling error component. If the contribution to σ_E^2 from retrieval errors can be neglected, the satellite estimates $\hat{R}_i$ for each overpass can be treated statistically as if they were exact. In Eq. (2.3) we can then set $\hat{R}_i = R_i \equiv R_{A_i}(t_i)$ and compute the sampling error component using (2.5). We will return to these assumptions later.

As we have already mentioned, the sampling error can depend on the local rainfall statistics as well as sampling characteristics of the satellite. A simple model for this dependence is based on the straightforward assumption that variations in

the total rainfall amount in an area are primarily due to variations in the number of independently evolving precipitating systems present within it rather than variations in the intensity of the individual systems. Such an assumption is present in almost all statistical treatments of rainfall, and some such assumption can be used to justify rain algorithms that estimate areal rainfall from areal coverage. The assumption is dynamically plausible because the convective cores of storms are quickly evolving small-scale phenomena, limited in their development by local lapse rates and the availability of moisture. Synoptic-scale lower-level convergence may affect the probability of convective plumes forming, but once started, they are self-limiting.

Starting from this simple assumption, BK00 obtained the formula

$$\frac{\sigma_E}{R} = C(RAS)^{-1/2}\,, \tag{2.6}$$

where

$$S = \sum_{i=1}^{n} A_i/A \tag{2.7}$$

is the "effective" number of full area sweeps of the grid box A by the satellite instrument swaths, and the prefactor C depends only weakly on a variety of rainfall characteristics consistent with a given value of the mean rain rate R, as described below. Arguments for a $1/\sqrt{R}$-dependence of relative sampling error on rain rate like that in Eq. (2.6) were given in BK96, who noted some evidence for it when estimates from simulations with radar data over southern coastal Japan (Oki and Sumi 1994) were plotted versus R. An extensive discussion of the dependence of sampling error on rain rate R is given by Huffman (1997). Quartly et al. (1999) provide a clear review of arguments for (2.6) and an example of an interesting application of these ideas to a rain climatology developed with data from the TOPEX/POSEIDON satellite dual-frequency altimeter.

Numerous estimates of rms sampling error have been made in the literature using simulated satellite sampling of data taken by ground-based measurement systems in a variety of geographical regions. BK00 examined many of these estimates, and found

that the dependence of σ_E/R on R was predicted quite well by (2.6) in those regions where data were available in sufficient quantities. In particular, as mentioned above, results of simulations with radar data over southern coastal Japan by Oki and Sumi (1994) agree quite well (BK96) with (2.6); and Steiner (1996) obtained error estimates using simulations with rain-gauge and radar data from Darwin and Melbourne, Florida and found that he could fit the dependence of error on R with an expression quite close to (2.6).

b. Model explanation

A simple model that gives the relationship (2.6) can now be described. A more thorough discussion is given by BK00. The model assumes that rainfall consists of individual uncorrelated rain events having, on average, area a and duration $2\tau_a$. From these assumptions they derived the expression

$$C = (ar_c)^{1/2}[1 - 2\tau_a/(T/S)]^{1/2} , \tag{2.8}$$

where $r_c = R/p$ is the mean nonzero rain rate in a satellite footprint (subscript c for "conditional"), p being the probability that a footprint contains nonzero rain. The ratio T/S can be thought of as the average time interval between two consecutive full area observations by the satellite. When the sampling is sparse, one has $T/S \gg 2\tau_a$, and in this limit $C \approx \sqrt{a\tau_c}$. When the effective sampling interval is comparable to τ_a, this simple cell model is no longer applicable, and one must employ a more accurate representation of the statistical properties of the local rain field, an example of which is described next.

A somewhat different explicit form of the constant C was derived by Bell et al. (1990) using an approach originally due to Laughlin (1981). Assuming that the entire area A is sampled at regular intervals $\Delta t = T/S$, they obtained the formula

$$\sigma_E^2 \approx (\sigma_A^2/S) f(\Delta t/2\tau_A) , \tag{2.9}$$

where σ_A^2 is the variance of the instantaneous rain rate $R_A(t)$,

$$\sigma_A^2 = \mathrm{var}[R_A(t)] \,, \tag{2.10}$$

τ_A is the corresponding correlation time [$(1/e)$- folding time of the autocorrelation of $R_A(t)$, assumed to be pure exponential], and with

$$f(\nu) = \coth \nu - 1/\nu. \tag{2.11}$$

The approximation (2.9) assumes $T \gg \tau_A$, which is certainly valid when T is of the order of 1 month, since τ_A is typically 4–10 h. The variance of the box-averaged rain rate σ_A^2 can, in turn, be expressed in the form

$$\sigma_A^2 = s^2 \Lambda^2 / A \,, \tag{2.12}$$

where s^2 is the variance of the instantaneous rain rate averaged over a satellite footprint. The quantity Λ^2 is the effective area of a rain fluctuation that can be considered as statistically independent of other such fluctuations within the grid box A, in analogy with the definition of an "effectively independent sample size" by Leith (1973). It is given by

$$\Lambda^2 = \frac{A}{N_0^2} \sum_{i=1}^{N_0} \sum_{j=1}^{N_0} \rho(|\mathbf{x}_i - \mathbf{x}_j|) \,, \tag{2.13}$$

where $\rho(z)$ denotes the spatial correlation between rain in two footprints separated by a distance z, N_0 is the total number of footprints in A, and the average is performed over all pairs of footprints. The length Λ can be thought of as the distance over which footprint-averaged rain rate is correlated, or as the typical size of a coherent rain event. Note that the value of Λ may in principle vary with both FOV size [which affects $\rho(z)$] and the area A, which affects the range of separations $|\mathbf{x}_i - \mathbf{x}_j|$ encountered in the double sum.

Combining equations (2.9) and (2.12), using the relations $R = pr_c$, and

$$s^2 = p s_c^2 + p(1-p) r_c^2 \tag{2.14}$$

$$\approx p(s_c^2 + r_c^2) \tag{2.15}$$

(the latter valid when p is small), one again obtains formula (2.6) for the sampling error, with the identification

$$C = \Lambda[r_c(1+\mu_c^2)]^{1/2} f(\Delta t/2\tau_A), \tag{2.16}$$

where r_c and s_c^2 are the mean and variance of nonzero rain rate (i.e., conditional on $R_{\rm FOV} > 0$), and $\mu_c \equiv s_c/r_c$. It should be pointed out that although the quantities p, r_c, s_c, and Λ may each depend strongly on the footprint size, our simple theory leads to the expectation that expressions (2.8) or (2.16) determining the constant C are insensitive to it. Short et al. (1993) have suggested that the ratio $\mu_c = s_c/r_c$ is relatively constant over a range of footprint sizes, averaging times, types of data (rain-gauge or radar) and climates. In the limit of sparse sampling this would imply

$$C \approx \text{const} \times r_c^{1/2}\Lambda\ , \tag{2.17}$$

which should be compared to (2.8). Note that unless A is much larger than a typical rain event, Λ^2 in (2.13) will depend non-trivially on A, and thereby change the A dependence of σ_E in (2.6). In fact, when A approaches the size of a single footprint, it is easy to see from (2.13) that $\Lambda^2 \approx A$.

3. Random error of monthly SSM/I rain rates

Rain estimates made from SSM/I observations provide a way of testing directly the validity of the proposed simple theory of sampling error. Coverage by the SSM/I as measured by S in (2.7) is quite close to that of TRMM's passive microwave sensor (TMI) for grid boxes at low latitudes, and so sampling errors should be similar in size, though their respective retrieval errors may differ. In this section we shall investigate the statistical behavior of the retrieved rain rates and the inferred statistics of random errors in gridded monthly averages of retrievals.

a. The SSM/I dataset

The dataset we used consists of rain data from two satellites, the F10 and F11, in nearly sun-synchronous polar orbits around the earth. The data were taken during the four-month Special Observing Period (SOP) of TOGA COARE from November 1992 to February 1993. Local visit times of the F10 and F11 during the SOP were roughly 9:30 am/pm and 5:30 am/pm respectively. The SSM/I on each satellite views a given spot on the earth an average of about 30 times per month, so that $S \approx 30$ in Eq. (2.6). (For the TRMM microwave instrument, $S \approx 30$ as well, but local visit times shift over the course of a month.)

Rain rates were derived using the Goddard Profiling Algorithm, which is based on the method described by Kummerow and Giglio (1994a,b), modified following the description given by Kummerow et al. (1996). The dataset was generated as part of the 3rd Algorithm Intercomparison Project (AIP-3), as described by Ebert et al. (1996), and in more detail by Ebert and Manton (1998). Rain rates are estimated for footprints which may be thought of as circles approximately 28 km in diameter, even though in reality they are elliptical in shape, the response of the microwave antenna is nonuniform over the FOV, and there is blurring due to the finite integration time of the SSM/I instruments. Kummerow and Giglio (1994b) provide a more detailed discussion of this topic. The retrieved rain rates are provided as successive arcs each containing 64 partially overlapping footprints and covering altogether a swath about 1400 km wide.

We study the statistics of rain in the region extending from 10° S to 10° N and from 135° E to 175° E in the tropical western Pacific. This region includes the area where the TOGA COARE Intensive Flux Array (IFA) was located. For an optimal choice of the grid-box size for our statistical analysis one needs to strike a compromise among several competing factors. The box needs to be large enough so that rain rates in neighboring boxes can be assumed to be statistically uncorrelated. This is essential for treating collections of grid-box averages as sets of statistically independent samples,

so that standard statistical methods of estimating confidence intervals for the averages can be used. On the other hand one would like the boxes to be small so that there are as many boxes as possible, thereby giving us a more detailed, smoother picture of the dependence of the retrieval statistics on local rain rate, as will be clear in the next section. A small box size also increases the likelihood that rain statistics within the box can be regarded as approximately homogenous. With these factors in mind we have chosen a grid-box size $A = 2.5° \times 2.5°$.

b. Estimate of the random error in grid-box averages

The SSM/I dataset itself does not provide access to the true monthly average rain rate $\bar{R}$ appearing in the definition of σ_E in Eq. (2.5). To circumvent this difficulty, we use a procedure suggested by Chang et al. (1993) to estimate the rms random error σ_E for either satellite. Consider the mean squared difference between the F10 and F11 estimates of a grid-box monthly average:

$$\begin{aligned} \langle(\hat{R}_{10} - \hat{R}_{11})^2\rangle &= \langle[(\hat{R}_{10} - \bar{R}) - (\hat{R}_{11} - \bar{R})]^2\rangle \\ &\approx \langle(\hat{R}_{10} - \bar{R})^2\rangle + \langle(\hat{R}_{11} - \bar{R})^2\rangle \\ &\approx 2\sigma_E^2 \,. \end{aligned} \tag{3.1}$$

The approximation above would be legitimate if the observations by the two satellites are far enough apart in time to be nearly uncorrelated. Although the legitimacy of this assumption may be surprising, since the satellites can in principle view the same scene only 4–5 hours apart, several factors appear to justify the approximation. Each satellite visits a grid box only once per day on average, and the visits of one satellite are generally well separated from the other's. Moreover, some simple calculations based on Laughlin's (1981) approach show that, for two satellites with idealized sampling like that of the F10 and F11, expression (3.1) is quite accurate, even though the two averages $\hat{R}_{10}$ and $\hat{R}_{11}$ are not in fact statistically independent. It should be noted, however, that the same calculation indicates that the approximation (3.1) is not so good

if the satellites were to have closer sampling times or, more surprisingly, respective visit times nearer to 12 hours apart. Finally, this approximation was corroborated by performing sampling error calculations using the method developed in BK96 and the exact sampling patterns of the F10 and F11 satellites, and the approximation (3.1) is borne out at the level of 5% accuracy.

The error variance σ_E^2 as estimated in (3.1) includes both the sampling error described in section 2 and also any contributions from randomly varying retrieval errors in the two satellites' estimates. As discussed in the previous section, if random retrieval errors are uncorrelated from footprint to footprint, the contribution to σ_E^2 from these errors should be quite small, and the sampling-error component would dominate the estimate of σ_E^2 based on (3.1). If, however, retrieval errors are correlated spatially or from one satellite viewing to the next, σ_E^2 may contain significant contributions from retrieval error. For any of the purposes reviewed in the introduction, though, the error σ_X^2 introduced there is more properly given by σ_E^2 rather than the sampling error for perfectly measured rain rates. The fact that the estimate σ_E^2 includes retrieval error as well as sampling error is therefore an advantage rather than a disadvantage to an approach using (3.1).

Systematic differences in the rain retrievals by the two satellites, if present, could also contribute to the estimates of σ_E^2 made with (3.1). Such differences might be due to instrumental biases or operational differences between the two systems, or to significant diurnal variation in the rain statistics for the grid box. The diurnal variation would, however, have to be more complex than a simple first-harmonic sinusoid in order to contribute in this way, since each satellite views grid boxes at two times of the day, twelve hours apart, on average. Differences in the F10 and F11 averages due to diurnal effects seem unlikely to be very large for grid boxes over oceanic regions, but could be appreciable for boxes containing significant amounts of land.

c. Statistical analysis of the data

Monthly averages of retrieved rain were obtained for each 2.5° × 2.5° grid box in the TOGA COARE SOP dataset described above, yielding a total of 512 samples (128 grid boxes, 4 months of data). Grid-box results were also segregated according to whether the grid boxes contain mostly land, mostly ocean, or a mixture, but the differences in the statistics for these subsets were, for the most part, difficult to discern. They will be discussed later.

The coverage provided by the two satellites can vary from grid box to grid box and month to month. To gauge this, let us define S_{10} and S_{11} as the effective numbers of full viewings of a grid box by the F10 and F11, respectively, as measured by (2.7). To compute S_{10} and S_{11}, a method is needed for estimating the areal fraction A_i/A for each satellite visit i.

(i) *Estimation of S_{10} and S_{11}.*

If the number of footprints required to cover the entire area A is known, the ratio of the actual number of footprints in A to the full-coverage number provides an estimate of the fraction A_i/A for that particular visit. A possible method of determining the full-coverage footprint number is to examine the distribution of the number of footprints observed in many overflights of a grid box. Since the SSM/I swath is wide compared to the grid-box size, we would expect a histogram of the number of footprints observed in a box to peak at the maximum possible number. In reality, such histograms are not so simply behaved. This is in part because the density of footprints varies with location in the instrument swath, being largest near the swath's edges. Sporadic data loss due to instrumental and algorithmic problems can also occur. As a result, the histogram of footprint counts displays a somewhat broadened peak at the largest footprint counts. Although a more exact method of determining the fractions A_i/A could certainly be devised, it is sufficient for our purposes to define the full-coverage footprint count as the

number of counts $N_{\max}$ where the histogram peaks. We estimate the fraction A_i/A for a given visit to a grid box to be the ratio of the actual footprint count to $N_{\max}$. This estimate can sometimes be greater or less than 1 even though the swath completely covers the grid box, but the monthly sums S_{10} and S_{11} that result from this choice are reasonably good approximations to the values that would be obtained from more geometric estimates, and in addition take account of occasional data dropouts. For the SSM/I dataset we found $N_{\max} \approx 120$. Values of S_{10} and S_{11} computed this way for the 512 cases ranged between 15 and 34, with a mean value of about 28, indicating considerable variations in the satellite sampling. (It should be noted that the number of days available in the months also varies.)

(ii) *Removing effects of variable coverage.*

Since our chief concern here is with how well (2.6) predicts the dependence of σ_E on local rain rate, it would be preferable if we could minimize the effects on our analysis of the varying coverage by the satellites. Arguments very similar to those used in deriving (2.6) predict

$$\langle(\hat{R}_{10} - \hat{R}_{11})^2\rangle = C^2 \frac{R}{A}\left(\frac{1}{S_{10}} + \frac{1}{S_{11}}\right), \tag{3.2}$$

where S_{10} and S_{11} are the effective numbers of full viewings of a grid box by the F10 and F11, respectively, as measured by (2.7). By defining a "mean" coverage S for the two satellites by

$$2/S = 1/S_{10} + 1/S_{11}\ , \tag{3.3}$$

we can recast Eq. (3.2) in a form identical to Eq. (2.6) even if the relative coverage by the two satellites varies. As in Eq. (2.6), the coefficient C in (3.2) may depend on local rain statistics in ways suggested by Eqs. (2.8) or (2.16), but it should be relatively insensitive to changes in coverages S_{10} or S_{11}. (It should be noted that the rain statistics determining C are now those of the "measured" rain, including the effects of randomly varying retrieval error.)

Consider the result of multiplying Eq. (3.2) by $S/2$,

$$S\langle(\hat{R}_{10} - \hat{R}_{11})^2\rangle/2 = C^2R/A\ . \tag{3.4}$$

The ensemble average $\langle\cdot\rangle$ here indicates an average over many different sequences of rain events all having the same monthly mean R and observed by the two satellites. Since changes in S have relatively little effect on the right-hand side of (3.4), the left-hand side will be insensitive to changes in S as well. This allows us to obtain estimates of the right-hand side of Eq. (3.4) from averages of data with differing values of S, so that we can write

$$C^2R/A = \langle S(\hat{R}_{10} - \hat{R}_{11})^2\rangle/2\ . \tag{3.5}$$

where now the angular brackets are meant to indicate an average over an ensemble of months with varying rain sequences with monthly average R *and* varying satellite sampling as measured by S.

(iii) *Dependence of RMS error on R.*

Guided by Eq. (3.5), then, we investigate the dependence of σ_E^2 on rain rate by first computing the mean rain rate

$$\hat{R} = (\hat{R}_{10} + \hat{R}_{11})/2 \tag{3.6}$$

for each of the 512 grid boxes and months. The 512 pairs of estimates from the F10 and F11 are sorted into 8 bins in order of increasing values of $\hat{R}$, with 64 samples to a bin. For each bin, an average over the 64 values of $S(\hat{R}_{10} - \hat{R}_{11})^2/2$ gives us an estimate of C^2R/A, using (3.5), at the mean R for that bin. The binning process destroys information regarding the geographical location of a particular box and the observation month—samples containing similar monthly averaged rain rates are lumped together regardless of their location or time of observation. Although rain statistics no doubt change as various factors affecting the formation and development of precipitating systems within each grid box change, the operating assumption is the same as that of

the simple model: that if the frequency with which rain events occur in a grid box is known, all other rain statistics at that location can be predicted reasonably well.

It was mentioned in section 2 that sampling errors for monthly averaged TRMM TMI data have been estimated with simulations using ground-based measurements in a variety of rain environments. Near the equator the TMI and a DMSP satellite carrying SSM/I provide almost identical coverage, as measured by S, if both instruments are providing rain estimates from the entire instrument swaths during the month. With perfect coverage, $S \approx 30$ for both satellites. In order to compare our SSM/I results to these earlier TRMM studies, Eq. (2.6) and our estimates of C^2R/A from (3.5) can be used to compute what the random error σ_E in monthly averages of SSM/I data would be for the same coverage $S_0 = 30$ assumed in the TRMM studies, via

$$\sigma_E = \left[\frac{\langle S(\hat{R}_{10} - \hat{R}_{11})^2\rangle/2}{S_0}\right]^{1/2}. \tag{3.7}$$

Figure 1 shows a plot of σ_E/R estimated for a single SSM/I providing maximum possible coverage during a month (i.e., assuming an average of 30 visits per month). Results are plotted versus the average R for each bin. Error bars are 95% confidence limits obtained under the assumption that differences in monthly means behave statistically like independent, normally distributed variables.

Also shown in Fig. 1 are sampling-error estimates based on two radar datasets collected from ships stationed over open ocean. The two estimates labeled "GATE" use the statistics of data taken over the eastern tropical Atlantic during Phases I and II of the Global-Atmospheric-Research-Program Atlantic Tropical Experiment (GATE) in 1974. The six estimates labeled "TOGA COARE" use the statistics of radar data from two ships during the three cruises of the SOP. The methods used in obtaining these estimates are described fully in BK00. Comparison of the SSM/I estimates with the TOGA COARE estimates is particularly appropriate because the data were taken during the same four months, although the radar data cover only a limited region around 2°S, 156°E.

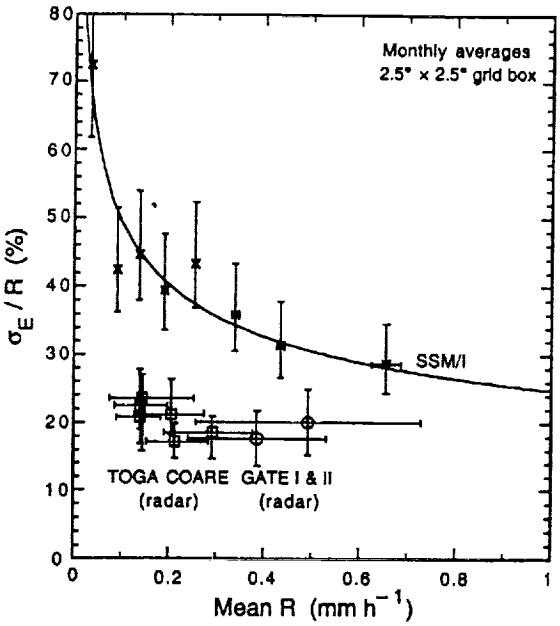

Figure 1. Relative sampling error of monthly grid-box averages over the equatorial western Pacific as a function of mean local rain rate R. SSM/I estimates have been corrected for missing data. A power-law fit is shown. Estimates using surface radar data assume coverage identical to what is provided by the TRMM microwave instrument, averaging 30 visits per month, very close to the SSM/I sampling. GATE radar data were taken during 1974. TOGA COARE radar data were taken contemporaneously with the SSM/I data.

Figure 1 brings out two salient characteristics of the SSM/I error estimates: 1) Estimated errors in SSM/I averages, which may include random retrieval errors, are 30% or more of monthly mean rain rates, and considerably larger than previous error estimates based on surface radar data, which are nominally estimates of sampling error alone (but could include the effects of errors in the radar-derived rain rates); and 2) even though both the simple model and experience (though admittedly limited) with ground-based data suggest that σ_E/R might be described by a power law with exponent $-1/2$, the SSM/I errors are better described by a power law with an exponent of about -0.3.

It should be noted that a number of sampling error estimates have been made with ground-based data other than those shown in Fig. 1. They are reviewed by BK00.

Two extensive studies, by Oki and Sumi (1994) and by Steiner (1996), yielded sampling-error estimates that are comparable in magnitude to the SSM/I values in Fig. 1, except at the highest rain rates, where the SSM/I estimates are larger. Because these studies used data from southern coastal Japan and from Darwin, on the northern coast of Australia, however, it is not clear that comparison with the SSM/I results is appropriate here. Rain in tropical coastal areas is quite different in character from rain over the open ocean. The SSM/I statistics we used are largely determined by rain over oceanic areas. The TOGA COARE radar statistics shown in Fig. 1 are from an area and time period included in the SSM/I dataset, and so would be most nearly comparable.

It is interesting to note that Chang et al. (1993) also obtained rms error as a function of the mean rain rate on a $5° \times 5°$ grid, using global oceanic monthly estimates of rainfall obtained with their microwave emission-based algorithm. If their results are converted to the format used here, they can be fitted to $\sigma_E/R \approx 0.26\,R^{-0.26}$ (R in mm h^{-1}). The relative errors they found are roughly 50% higher than the corresponding errors for $5° \times 5°$ boxes we found (not shown) using the SSM/I dataset studied here. We conjecture that, because the grid boxes in Chang et al.'s (1993) study were all $5° \times 5°$ regardless of location, boxes at higher latitudes that contributed to their statistics had smaller physical areas, and Eq. (2.6) predicts that they would have higher rms errors than for boxes near the equator. Thus, the higher errors of extra-tropical grid boxes may have been averaged with the errors for tropical grid boxes and resulted in an overall increase in average error, whereas our analysis covers only equatorial areas.

Figure 1 has shown that, where they can be compared, the statistics of the microwave-retrieved rain rates clearly differ in important ways from the statistics of surface radar data. In the sections that follow we shall try to identify where the differences occur, propose some useful diagnostics for these differences, and suggest how Eq. (2.6) might be modified to take them into account.

4. Exploration of ground-radar–SSM/I differences

The assumptions of the simple model in section 2 lead to predictions for sampling error like Eq. (2.9), where mean squared error is the product of the variance of area-averaged rain rate, σ_A^2, and a factor $f(\Delta t/2\tau_A)/S$ determined by the temporal sampling pattern of the satellite and by the correlation time τ_A of area-averaged rain rate. We can rewrite it somewhat schematically as

$$\sigma_E^2 \approx \sigma_A^2 f(T/2\tau_A S)/S \; . \tag{4.1}$$

In reality, when satellite visits are not evenly spaced and the area A is not viewed in its entirety on each visit, the dependence of f/S on a satellite's sampling pattern is more complicated than the simple dependence on S in (4.1) suggests. Based on an earlier study (BK96) with TRMM sampling, however, Eq. (4.1) seems to capture much of the change in sampling error with satellite sampling.

As we shall see later, the correlation times of SSM/I-retrieved rain rates tend to be similar in size to the correlation times seen in radar data and small compared to the typical time interval between SSM/I visits. We therefore conclude that the factor f cannot explain the differences in sampling errors in Fig. 1. Most of the difference seems to be due to differences in variability of area-averaged rain rate as reported by satellite and ground-based systems, and we turn now to investigating the differences in σ_A^2 for the two.

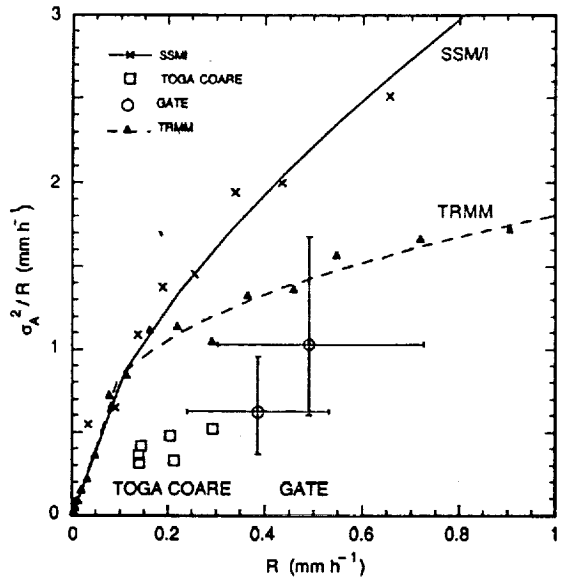

Figure 2. Ratio of the variance of instantaneous area-averaged rain rate $R_A(t)$ to R, $A = 2.5° \times 2.5°$, computed following the procedures used for Fig. 1. The simple model predicts that this quantity should be insensitive to local rain rate. Error bars (95% conf.) are shown only for GATE, but others would have similar errors. A power-law fit to the SSM/I points is shown. Corresponding statistics derived from TRMM TMI data are also plotted, and are discussed in Sec. 6.

By combining Eqs. (2.6) and (2.9) it is easy to show that the simple model predicts that σ_A^2 should increase linearly with R, so that the ratio σ_A^2/R should remain constant with changing local rain rates. Fig. 2 shows this quantity plotted as a function of R using the same binning procedure as in Fig. 1. In order to improve the legibility of the figure, only error bars (95% confidence intervals) for the ratio computed from GATE radar data are shown. They are representative of the estimated errors in the other plotted quantities. (Also shown are corresponding values obtained from TRMM TMI retrievals. These will be discussed later.) Given the level of uncertainty, it could be argued that the surface radar statistics are consistent with the constancy with R predicted by the simple model, though synoptic conditions at the two radar sites are sufficiently different that some underlying changes in the statistics may also be occurring. Whether or not this is so, it is evident from Fig. 2 that variances in SSM/I

area averages are significantly larger than for the same averages obtained with surface radar, and they also appear to increase faster with R than the surface data.

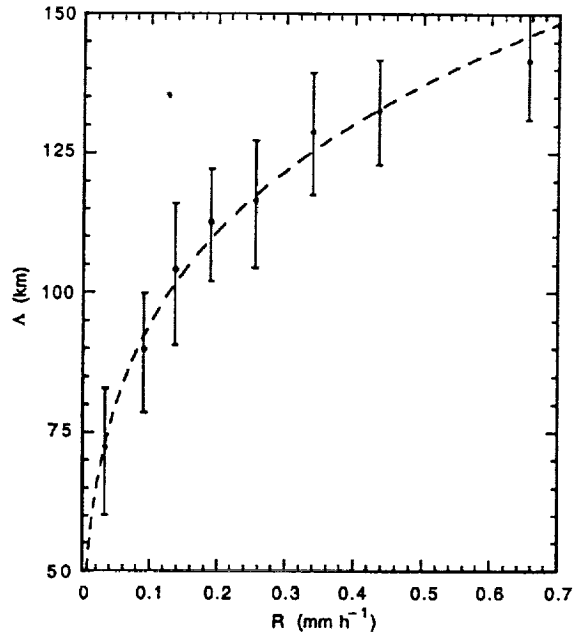

Figure 3. The scale of "statistically independent rain events," for SSM/I data in 2.5° × 2.5° grid boxes, from Eq. (2.13). If spatial correlations decreased exponentially as $\exp(-z/\lambda)$ *with separation* z *and the dimensions of* A *are large compared to* λ*, then* $\lambda = \Lambda/\sqrt{2\pi}$*. See appendix for details.*

Equation (2.12) indicates that σ_A^2 is determined by the variance of the individual SSM/I "point" estimates of rain rate (i.e., s^2 for FOV estimates) and by Λ^2, the area of statistically independent rain events. Figure 3 shows the dependence of Λ on R, calculated using Eq. (2.13). The calculation of Λ had to be adapted to handle the actual spatial distribution of SSM/I footprints, and is described in the appendix. In this and the plots that follow, the statistics for each value of R are averages over 64 grid-box/months with monthly means in the neighborhood of R, just as in Figs. 1 and 2. SSM/I estimates for regions with monthly rain rates similar to those observed by the surface radar in TOGA COARE, $R \approx 0.2\,\mathrm{mm\,h^{-1}}$, yield values of $\Lambda \approx 100$ km (corresponding to a "correlation distance" of about 40 km—see appendix). If the TOGA COARE radar data are smoothed to a spatial resolution corresponding to the

scale of the SSM/I footprint area, about $\sqrt{\pi}(28/2) \approx 25\,\mathrm{km}$, and used to calculate Λ, a value of Λ very close to the SSM/I value is obtained. It is therefore the larger values of s^2 for the SSM/I rather than differences in Λ that are mostly responsible for the larger values of σ_A^2 seen in Fig. 2.

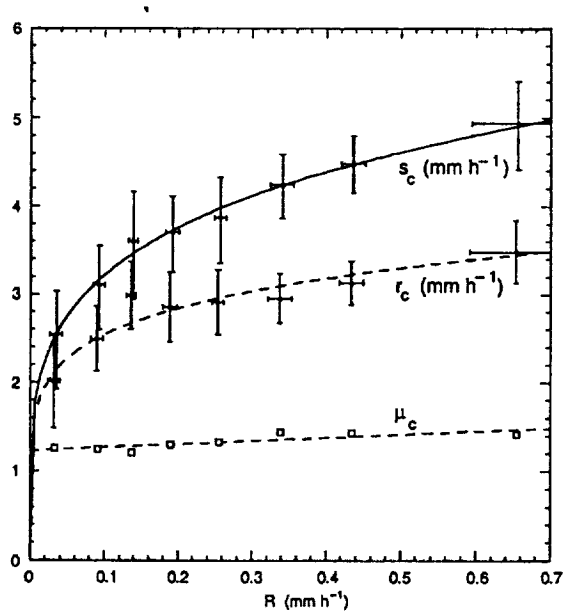

Figure 4. Mean r_c and standard deviation s_c of SSM/I rain rates in FOVs with nonzero rain, and the ratio $\mu_c = s_c/r_c$.

Equation (2.15) relates values of s^2 to the average areal coverage by rain, p, and the mean and variance of nonzero rain rates, r_c and s_c^2. Figure 4 shows the conditional mean $r_c = R/p$ and standard deviation s_c of nonzero rain seen by SSM/I, and also the ratio $\mu_c = s_c/r_c$, as a function of R. The statistics are comparable in size to those reported for GATE data by Short et al. (1993), especially μ_c. The ratio μ_c is nearly constant, a phenomenon also noted by Short et al. (1993) in other rain data. There are, however, subtle threshold-dependent effects in the conditional statistics that make intercomparison of the radar and SSM/I statistics problematic. The radar is able to detect much smaller rain rates than the SSM/I. When values of r_c, s_c, and μ_c are calculated from surface TOGA COARE radar data smoothed to a spatial resolution corresponding to the scale of an SSM/I FOV [$\approx (25\ \mathrm{km})^2$], we find values

$r_c = 0.5$ mm h^{-1}, $s_c = 1.4$ mm h^{-1}, and $\mu_c = 2.7 \pm 0.3$. They are quite different from the satellite values. For example, we see in Fig. 4 that for the SSM/I data μ_c ranges between 1.21 and 1.44. The difference in the values of μ_c obtained by us from TOGA COARE radar data and the values obtained from SSM/I data and in the analyses of surface data by others suggests that μ_c may depend on the threshold of detectability of rain in a way that was fortuitously absent in other studies.

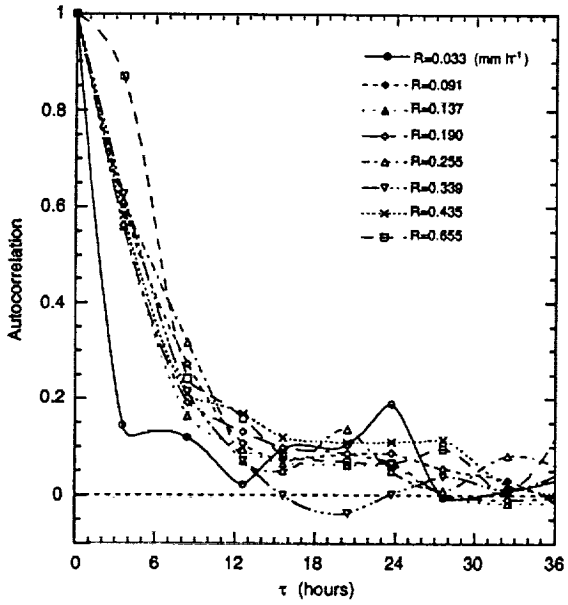

Figure 5. Autocorrelation of SSM/I rain rate averaged over 2.5° × 2.5° grid boxes for various categories of monthly rain rate R. Correlations are shown only when more than about 400 pairs of observations are available at a given separation τ. Curves through data points are smoothed interpolations.

In order to study temporal correlations of area-averaged SSM/I rain estimates, a time series of the average rain rate for full-area observations at each grid-box location was obtained. All visits with greater than about 85% coverage, determined from the footprint counts as explained in section 3.c.i, were included to get a time series that is sufficiently dense. Because the visit times of the F10 and F11 sometimes differed by as little as 3 h, these series had sufficient time resolution for useful time correlations to be obtained. Figure 5 shows the lagged autocorrelations of $R_A(t)$ sorted into the same 8 climatological rain-rate bins used in the previous figures; that is,

autocorrelations for a given R represent the statistics of 64 time series with monthly means in the neighborhood of R. For each of the 8 rain-rate categories we fitted the lagged autocorrelation function of the area-averaged rain rate to a simple exponential form $\exp(-|t - t'|/\tau_A)$. The correlation times τ_A were found to be about 6 hours and nearly independent of R, except at the lowest and highest rain rates. Spectral analysis of the time series indicated enhanced spectral power at frequencies corresponding to periods of 2–5 days and 40–50 days. The former may possibly be related to the convective disturbances with that time scale discussed by Takayabu and Nitta (1993), while the latter may be related to the Madden–Julian oscillation (Madden and Julian 1972; Chen and Yanai 2000).

It is well known that the statistical behavior of rainfall differs over land and ocean. To investigate this quantitatively, we employed a land/ocean mask at 2.5° spatial resolution. Of the 128 grid boxes in the chosen area, 97 are categorized as covered by ocean, 23 as mostly covered by land—largely concentrated around New Guinea in the southwest quadrant of the area we studied—and 8 as containing substantial amounts of both. The statistics of land-containing grid boxes were sorted into only 4 bins with increasing rain rates R in order to have a reasonable number of samples in each bin. Monthly rain rates in the land-containing boxes tended to range over values less than half as large as for the ocean-covered boxes. Most land–ocean differences in the statistics were indistinguishable from variability caused by small-sample effects. The conditional means r_c, however, were 50% to 75% larger over land, unlike the values of s_c, which were, perhaps surprisingly, a little smaller. The ratio μ_c ranged from 1.43 to 1.56 over ocean and from 0.85 to 1.0 over land. A pronounced peak in spectral power was found in the time spectrum of rain over land-covered boxes at a frequency of 1 day^{-1}, indicating the presence of a strong diurnal cycle. No spectral peak was evident in oceanic rain rates at that frequency. There is also little sign of any enhanced autocorrelation at $\tau = 24\,\text{h}$ in Fig. 5, except perhaps for grid boxes with the smallest

rain rates, indicating that statistics tended to be dominated by the statistics of the oceanic grid boxes.

5. Power-law descriptions of SSM/I statistics

The statistics of the SSM/I retrieved rain rates are described quite well by simple power-law dependences on R, as can be seen from the power-law fits shown in Figs. 1–4. Since this provides a much more concise description of the statistics, we present these results here.

It is convenient to express the various statistical quantities as powers of the dimensionless quantity p rather than R. We introduce the three basic exponents α, β and γ through the relations

$$r_c = r_0 p^\alpha, \quad s_c^2 = s_0^2 p^\beta, \quad \Lambda^2 = \Lambda_0^2 p^\gamma \, . \tag{5.1}$$

Note that in the simple model all the exponents would vanish. From the definition $R = p r_c$ it follows that

$$R = r_0 p^{1+\alpha}, \tag{5.2}$$

and if we treat the ratio μ_c as approximately constant, Eq. (2.15) gives

$$s^2 \approx (s_0^2 + r_0^2) p^{1+\beta} \, . \tag{5.3}$$

(Strict constancy of μ_c would imply $\beta = 2\alpha$.)

The expression (2.12) for σ_A^2 implies the power-law relation

$$\sigma_A^2 = (s_0^2 + r_0^2)(\Lambda_0^2/A) p^{1+\beta+\gamma}. \tag{5.4}$$

Because p and R are related by (5.2), the exponents α, β, and γ can be derived from the exponents obtained with error-weighted least-squares power-law fits to the statistics in Figs. 2–4. We find that the SSM/I statistics can be reasonably well explained by the values

$$\alpha = 0.17, \quad \beta = 0.53, \quad \gamma = 0.53. \tag{5.5}$$

The coefficients of the power-law fits in Eqs. (5.1) were found to be

$$r_0 = 4.5 \text{ mm h}^{-1},\ s_0 = 7.6 \text{ mm h}^{-1},\ \Lambda_0 = 220 \text{ km} . \tag{5.6}$$

Although not shown here, it was found that the right-hand side of Eq. (3.5) is proportional to σ_A^2 to reasonably good accuracy; that is, the dependence of σ_E on R is mostly determined by the R-dependence of σ_A, as predicted in (4.1). Their relationship is described empirically by

$$\sigma_E^2 = 0.66\,\sigma_A^2/S . \tag{5.7}$$

It is interesting to compare the empirical coefficient in (5.7) with what would be estimated from Eqs. (2.9) and (2.11). If we use the correlation time $\tau_A = 6\,\text{h}$ found in section 4 for most rain rates R, and the mean monthly areal coverage $S = 28$, we calculate $f(T/2\tau_A S) = 0.56$. Given the crude nature of the estimate, which assumes exponential autocorrelation of $R_A(t)$ and equally spaced observations in time by the satellite, the extent of agreement with the observed value 0.66 is remarkable.

If the relatively small effects on sampling error σ_E due to changes in τ_A with R are neglected, Eq. (4.1) implies

$$\sigma_E^2 \propto p^{1+\beta+\gamma}. \tag{5.8}$$

The relative sampling error for a single SSM/I satellite shown in Fig. 1, when fitted to a power law in R,

$$\sigma_E/R \propto R^{\delta} , \tag{5.9}$$

gives an exponent $\delta = -0.30$ (instead of -0.5 predicted by the simple model). The power laws (5.1) would predict $\delta = -1/2 + (\beta + \gamma - \alpha)/2(1 + \alpha)$, or $\delta = -0.12$ when the exponents in (5.5) are substituted. The discrepancy in the exponent obtained by directly fitting σ_E/R to a power law and the exponent predicted using the other empirical exponents appears to be due to the changes in the correlation time of $R_A(t)$ at the smallest and largest rain rates R seen in Fig. 5. The resulting changes in the factor

f in (4.1) are equivalent to an increase in the predicted value of δ from –0.12 to a value near -0.3.

6. Some Preliminary TRMM Results

The analysis so far described was motivated in part by the need to supply a measure of the random error for gridded monthly rain-rate products produced by TRMM. From a rainfall-retrieval-algorithm point of view, the TRMM's TMI has an advantage over the SSM/I because the TRMM satellite orbits closer to the earth, giving the instruments improved spatial resolution, and the TMI includes a lower-frequency dual-polarization 10.7-GHz channel in addition to SSM/I's four higher-frequency channels. Although the random error in TRMM monthly rain climatologies will be more thoroughly explored in a subsequent paper, it is interesting to compare the performance of TRMM to what has been learned about SSM/I here.

a. TRMM Data

We used TMI surface rainfall retrievals made available by the Goddard Space Flight Center (GSFC) Distributed Active Archive Center (DAAC) as official TRMM product 2A12, version 4, for the four-month period January–April 1998 over the same geographical area as the one used in the SSM/I study here. The TMI rain product has benefited not only from the instrumental advantages mentioned above, but also from the use of a version of the algorithm more advanced than the one used with the SSM/I data. The most important change in the algorithm is probably the addition of a step which adjusts for the relative amounts of convective and stratiform rain present in each FOV, as described by Hong et al. (1999).

b. Data Analysis Results

The dependence of the statistics of TMI rain-rate data on local rain rate R was determined in the same manner as before, by binning the statistics for each 2.5° × 2.5° grid box and month according to the monthly mean R. A plot of σ_A^2/R for TRMM

is shown in Fig. 2. The number of bins was increased to 16 when it became apparent that the statistics change in character above and below $R \sim 0.1$ mm h^{-1}, so that each point represents an average of 32 rather than 64 grid-box results. It is encouraging to see that the TRMM statistic has moved closer to the radar values. The improvement is especially marked at the higher rain rates, where the ratio is both more nearly constant with R and considerably lower than the SSM/I results.

Rather good fits of the TRMM results to power laws in R can be obtained if a fairly sharp crossover of the exponent values for rain rates above and below $R = 0.1$ mm h^{-1} is allowed. The parameters of the fits in both regimes are given in Table 1. The parameters for the conditional rain statistics for TRMM are very different from those of the SSM/I statistics given in (5.5) and (5.6).

7. Summary and Conclusions

SSM/I rain-rate data taken during the TOGA COARE experiment were used to estimate the random error in monthly averages over 2.5° grid boxes in the western tropical Pacific. The satellite algorithm that was used is a predecessor of the one currently used to process TRMM microwave data. The error estimates were made two different ways: one estimate was obtained from the rms differences of the monthly averaged rain rates given by the F10 and F11 satellites; a second estimate was obtained from the variance, σ_A^2, of instantaneous area-averaged rain rates $R_A(t)$, and a rough estimate of the temporal correlations of $R_A(t)$. The two estimates agreed quite well. This suggests that reasonable estimates of random error in gridded monthly averages might be made from σ_A^2 and an approximate characterization of the time correlations of $R_A(t)$—quantities that can be obtained from the satellite data themselves. Such estimates will include the contributions of random retrieval errors to the total error.

Over the ocean, both the magnitude of σ_A^2/R and its dependence on local rain rate R are clearly different for the SSM/I rain estimates and surface radar estimates. The higher variance of SSM/I estimates of $R_A(t)$ compared to radar appears to be due

mostly to the larger variance of individual footprint estimates, measured by s^2, rather than greater spatial correlations of the rain data—to the extent they are measured by Λ. It will be shown in a separate paper that the SSM/I estimates are highly correlated with stratiform rain as identified in the TOGA COARE surface radar data, and not so well correlated with rain identified as convective; the SSM/I rain estimates where there is stratiform rain are much larger than the corresponding radar estimates, whereas rain estimates where the radar reports convective rain tend to be estimated smaller by SSM/I. The net effect is to make s^2 large for SSM/I FOV estimates. These conclusions apply, of course, only to the rain data generated by the particular algorithm used to produce the dataset investigated here.

Little has been said here about how sampling error depends on the grid-box area A. As was seen in Eq. (2.6), the simple model would predict $\sigma_E \propto A^{-1/2}$. Equations (2.9) and (2.12), however, indicate that this is only true if the area A is much larger than Λ^2. The 2.5° × 2.5° boxes studied here are not quite large enough in this respect. Although increasing the box size to 5° × 5° reduces the number of samples per bin when the statistics are binned by rain rate R, as was done in section 3, such an experiment shows that the power-law dependence of σ_A^2 on R is almost the same for the two box sizes, but that the dependence of σ_A^2 on A is consistent with $\sigma_A \propto A^{-0.33}$ rather than with $A^{-1/2}$. Thus, increasing the box size from 2.5° to 5° does not decrease sampling error as much as the simple model would have predicted if A were larger.

Based on our results, it is recommended that future algorithm intercomparison projects include comparisons of σ_A^2/R for grid-box sizes of the order of 2.5° or larger, in addition to comparing the mean rain rates R themselves. The ratio is easy to calculate and, as has been shown here, can serve to bring out some aspects of the algorithms that can be missed in point-by-point comparisons but are important for climatological use of the data. This quantity has the advantage that, other things being equal, it is not so sensitive to instrument resolution, and so makes intercomparison of different

measurement systems conceptually easier. The quantity σ_A^2 can reveal the presence of correlated retrieval errors in the satellite product, a possible byproduct of the reason for its being larger in the SSM/I data than in the radar data, as will be discussed in a subsequent paper.

An especially important result is that the quantity σ_A^2 can be used to estimate the accuracy of monthly averages of rain data via a relation like Eq. (5.7). Such an estimate avoids some of the assumptions used in parameterizing error in terms of average rain rate R, though it requires that the satellite dataset supply values of σ_A as well as R for each grid box.

Whether because of better resolution and additional channels in the TMI or because of improvements in algorithms, the statistics of TRMM TMI (version 4) rain estimates from the western tropical Pacific appear to be significantly closer to oceanic surface radar statistics than the SSM/I statistics. An improved TMI algorithm is now being used to process TMI data, and we expect even better agreement with ground-based data. This will be examined in a future paper.

Acknowledgements. We wish to thank L. Giglio for his generous help in obtaining and using the SSM/I dataset, and Dr. Paul Kucera for his advice in using the TOGA COARE radar data. We have benefitted from many helpful discussions about TMI data with Drs. Ye Hong and William S. Olson. This research was supported by the Office of Earth Science of the National Aeronautics and Space Administration as part of the Tropical Rainfall Measuring Mission.

APPENDIX

Computation of the Length Scale Λ

In this appendix we discuss in more detail the computation and interpretation of Λ^2 defined in Eq. (2.13). It is helpful in developing an interpretation of Λ to assume that the footprints are sufficiently densely and evenly distributed that they can be

treated as if arranged in a regular rectangular array completely filling the area $A = L^2$. Each footprint occupies a box of side $d = L/N$. The number of footprints is then $N_0 = N^2$. The quantity Λ so defined in general depends both on the area size L and the footprint size d. For instance, if the area is small enough to be covered by a single footprint, then obviously $\Lambda = L$. More generally, however, Λ is closely related to the scale over which the data are spatially correlated, as we now show.

Using the identity

$$\sum_{i=1}^{N}\sum_{j=1}^{N} f(i-j) = \sum_{m=-N}^{N} (N-|m|)f(m) \tag{A1}$$

for a function $f(i)$ defined at each integer i, $|i| \leq N-1$, we can write (2.13) as

$$\begin{aligned}\Lambda^2 &= \frac{A}{N^4}\sum_{i,j=1}^{N}\sum_{k,l=1}^{N}\rho(|\mathbf{x}_{ij}-\mathbf{x}_{kl}|) \\ &= \frac{A}{N^4}\sum_{m_1=-N}^{N}\sum_{m_2=-N}^{N}(N-|m_1|)(N-|m_2|)\rho(|\mathbf{m}|d)\end{aligned} \tag{A.2}$$

This formally transforms the sum over the correlation between all pairs of footprints in the $N \times N$ array into a weighted sum of the correlation between each footprint in an equally spaced $(2N+1) \times (2N+1)$ array and a footprint located at the center of the array. If $\rho(|\mathbf{m}|d)$ is sufficiently smooth, Eq. (A.2) can be treated as a discrete numerical approximation to a continuous double integral. The approximation becomes exact in the limit $d \to 0$ ("point footprint"). Introducing the separation vector $\mathbf{s} = \mathbf{m}d$, and using the relations $A = L^2$ and $L = Nd$ we can express Λ^2 in this limit as an area integral over a $2L \times 2L$ square:

$$\Lambda^2 \approx \frac{1}{L^2}\int_{-L}^{L} ds_1 \int_{-L}^{L} ds_2 (L-|s_1|)(L-|s_2|)\rho(|\mathbf{s}|) \; .$$

By going to polar coordinates this can be reduced further to the one-dimensional integral

$$\Lambda^2 = 4\int_0^{\sqrt{2}L} s g(s)\rho(s) ds \tag{A3}$$

with the angular integral replaced by the areal weighting factor

$$g(s) = \int_{\varphi_0(s)}^{\varphi_1(s)} d\varphi (1 - \frac{s}{L}\cos\varphi)(1 - \frac{s}{L}\sin\varphi), \tag{A4}$$

where

$$\varphi_0(s) = \begin{cases} 0, & s \le L; \\ \cos^{-1}(L/s), & s > L; \end{cases}$$

and

$$\varphi_1(s) = \pi/2 - \varphi_0(s) \, .$$

Carrying out the integrations in (A4) we get

$$g(s) = \begin{cases} \pi/2 - 2s/L + s^2/(2L^2), & 0 \le s \le L; \\ \pi/2 - 1 - 2\cos^{-1}(L/s) + 2\sqrt{(s^2/L^2 - 1)} - s^2/(2L^2), & L < s \le \sqrt{2}L \, . \end{cases}$$

When the footprints are small compared with spatial correlation lengths and the grid-box size A is large, one can easily show that

$$\Lambda^2 \rightarrow 2\pi L_{\rm int}^2 \, , \tag{A5}$$

where

$$L_{\rm int} = \int_0^\infty s\rho(s)ds \tag{A6}$$

is an "integral correlation length" which is just the usual correlation length, the $(1/e)$-folding distance, if the correlation $\rho(s)$ decreases exponentially.

Although the continuous integral representation of Λ^2 given by Eq. (A3) in the limit of infinite resolution is conceptually illuminating, estimation of the integral from the finite resolution data in practice takes one back to a discrete sum. We estimated Λ^2 for each 2.5° grid-box area as follows: The footprint pairs are binned according to their mutual distance of separation in units of $d/2$ where d is the nominal diameter of an SSM/I footprint (about 28 km). For all the pairs belonging to the k-th separation bin ($k = 0, 1, 2, \ldots, k_{\rm max} = [2\sqrt{2}L/d]$, where $[x]$ denotes the integer part of x) we compute the correlation coefficient ρ_k, the mean separation $\bar{s}_k$ and the angular factor

$g_k = g(kd/2)$. In terms of these quantities a reasonably accurate estimate of Λ^2 is given by the Riemann-sum approximation

$$4 \sum_{k=0}^{k_{max}} \frac{1}{2}(\rho_{k+1}\bar{s}_{k+1}g_{k+1} - \rho_k \bar{s}_k g_k)(\bar{s}_{k+1} - \bar{s}_k).$$

This method of proceeding does not require the assumption that the footprints be uniformly distributed in the area A that was used to develop the interpretation (A3) for Λ. We have tested the accuracy of the approximation by plotting $s^2\Lambda^2/A$ against σ_A^2. Our results are closely fitted by a straight line with unit slope.

REFERENCES

Bell, T. L., A. Abdullah, R. L. Martin and G. R. North, 1990: Sampling errors for satellite-derived tropical rainfall: Monte Carlo study using a space–time stochastic model. *J. Geophys. Res.*, **95 D**, 2195–2205.

——, and P. K. Kundu, 1996: A study of the sampling error in satellite rainfall estimates using optimal averaging of data and a stochastic model. *J. Climate*, **9**, 1251–1268.

——, and ——, 2000: Dependence of satellite sampling error on monthly averaged rain rates: Comparison of simple models and recent studies. *J. Climate*, **13**, 449–462.

Chang, A. T. C., L. S. Chiu, T. T. Wilheit, 1993: Random errors of oceanic monthly rainfall derived from SSM/I using probability distribution functions. *Mon. Wea. Rev.*, **121**, 2351–2354.

Chen, B., and M. Yanai, 2000: Comparison of the Madden-Julian oscillation (MJO) during the TOGA COARE IOP with a 15-year climatology. *J. Geophys. Res.*, **105 D**, 2139–2149.

Ebert, E. E., M. J. Manton, P. A. Arkin, R. J. Allam, G. E. Holpin, and A. Gruber, 1996: Results from the GPCP Algorithm Intercomparison Projects. *Bull. Amer. Meteor. Soc.*, **77**, 2875–2887.

——, and ——, 1998: Performance of satellite rainfall estimation algorithms during TOGA COARE. *J. Atmos. Sci.*, **55**, 1537–1557.

Hong, Y., C. D. Kummerow, and W. S. Olson, 1999: Separation of convective and stratiform precipitation using microwave brightness temperature. *J. Appl. Meteor.*, **38**, 1195–1213.

Huffman, G. J., 1997: Estimates of root-mean-square random error for finite samples of estimated precipitation. *J. Appl. Meteor.*, **36**, 1191–1201.

Kummerow, C., and L. Giglio, 1994a: A passive microwave technique for estimating rainfall and vertical structure information from space. Part I: Algorithm description. *J. Appl. Meteor.*, **33**, 3–18.

——, and ——, 1994b: A passive microwave technique for estimating rainfall and vertical structure information from space. Part II: Applications to SSM/I data. *J. Appl. Meteor.*, **33**, 19–34.

——, W. S. Olson, and L. Giglio, 1996: A simplified scheme for obtaining precipitation and vertical hydrometeor profiles from passive microwave sensors. *IEEE Trans. Geosci. Remote Sensing.*, **34**, 1213–1232.

——, W. Barnes, T. Kozu, J. Shiue, and J. Simpson, 1998: The Tropical Rainfall Measuring Mission (TRMM) sensor package. *J. Atmos. Ocean Tech.*, **15**, 808–816.

Laughlin, C. R., 1981: On the effect of temporal sampling on the observation of mean rainfall. *Precipitation Measurements from Space, Workshop Report.* D. Atlas and O.W. Thiele, Eds. NASA Publ., available from Goddard Space Flight Center, Greenbelt, MD 20771.

Leith, C. E., 1973: The standard error of time-average estimates of climatic means, *J. Appl. Meteorol.*,**12**, 1066–1069.

Madden, R. A., and P. R. Julian, 1972: Description of global-scale circulation cells in the tropics with a 40–50 day period. *J. Atmos. Sci.*, **29**, 1109–1123.

Oki, R., and A. Sumi, 1994: Sampling simulation of TRMM rainfall estimation using radar-AMeDAS composites. *J. Appl. Meteor.*, **33**, 1597–1608.

Quartly, G. D., M.A. Srokosz, and T.H. Guymer, 1999: Global precipitation statistics from dual-frequency TOPEX altimetry. *J. Geophys. Res.*, **D 104**, 31489–31516.

Short, D. A., D. B. Wolff, D. Rosenfeld, and D. Atlas, 1993: A study of the threshold method utilizing rain gauge data. *J. Appl. Meteor.*, **32**, 1379–1387.

Simpson, J., R. F. Adler, and G. R. North, 1988: A proposed tropical rainfall measuring mission satellite. *Bull. Amer. Meteor. Soc.*, **69**, 278–295.

——, C. Kummerow, W.-K. Tao, and R. F. Adler, 1996: On the Tropical Rainfall Measuring Mission (TRMM). *Meteorol. Atmos. Phys.*, **60**, 19–36.

Steiner, M., 1996: Uncertainty of estimates of monthly areal rainfall for temporally sparse remote observations. *Water Resources Res.*, **32**, 373–388.

Takayabu, Y. N., and T. Nitta, 1993: 3–5 day-period disturbances coupled with convection over the tropical Pacific ocean. *J. Meteor. Soc. Japan*, **71**, 221–246.

Taylor, J. R., 1997: *An Introduction to Error Analysis. The Study of Uncertainties in Physical Measurements.* Univ. Science Books, Sausolito, California, 344 pp.

Wilheit, T. T., 1988: Error analysis for the Tropical Rainfall Measuring Mission (TRMM). *Tropical Rainfall Measurements*, J. S. Theon and N. Fugono, Eds., A. Deepak, 377–385.

Wilks, D. S., 1997: Resampling hypothesis tests for autocorrelated fields. *J. Climate*, **10**, 65-82.

Zwiers, F. W., 1990: The effect of serial correlation on statistical inferences made with resampling procedures. *J. Climate*, **3**, 1452–1461.

Figure Captions

FIG. 1. Relative sampling error of monthly grid-box averages over the equatorial western Pacific as a function of mean local rain rate R. SSM/I estimates have been corrected for missing data. A power-law fit is shown. Estimates using surface radar data assume coverage identical to what is provided by the TRMM microwave instrument, averaging 30 visits per month, very close to the SSM/I sampling. GATE radar data were taken during 1974. TOGA COARE radar data were taken contemporaneously with the SSM/I data.

FIG. 2. Ratio of the variance of instantaneous area-averaged rain rate $R_A(t)$ to R, $A = 2.5° \times 2.5°$, computed following the procedures used for Fig. 1. The simple model predicts that this quantity should be insensitive to local rain rate. Error bars (95% conf.) are shown only for GATE, but others would have similar errors. A power-law fit to the SSM/I points is shown. Corresponding statistics derived from TRMM TMI data are also plotted, and will be discussed in Sec. 6.

FIG. 3. The scale of "statistically independent rain events," for SSM/I data in 2.5° $\times$ 2.5° grid boxes, from Eq. (2.13). If spatial correlations decreased exponentially as $\exp(-z/\lambda)$ with separation z and the dimensions of A are large compared to λ, then $\lambda = \Lambda/\sqrt{2\pi}$. See appendix for details.

FIG. 4. Mean r_c and standard deviation s_c of SSM/I rain rates in FOVs with nonzero rain, and the ratio $\mu_c = s_c/r_c$.

FIG. 5. Autocorrelation of SSM/I rain rate averaged over 2.5° $\times$ 2.5° grid boxes for various categories of monthly rain rate R. Correlations are shown only when more than about 400 pairs of observations are available at a given separation τ. Curves through data points are smoothed interpolations.

Tables

TABLE 1. Power-law dependence of r_c, s_c, and Λ on p, defined in Eq. (5.1), and power-law dependence of σ_E/R on R defined in Eq. (5.9), for TRMM TMI statistics over the western tropical Pacific. As can be seen in Fig. 2, fits to the data must be obtained separately for small and large R.

	α	β	γ	δ	r_0 (mm h^{-1})	s_0 (mm h^{-1})	Λ_0 (km)
$R < 0.1$ mm h^{-1}	1.02	3.40	0.46	0.03	24.6	379	175
$R > 0.1$ mm h^{-1}	1.44	0.90	0.44	-0.34	104	14	165